Q. J. R. Meteorol. Soc. (1997), **123**, pp. 2349–2375

Mesoscale analysis of the activation of a cold front during cyclogenesis

By K. A. BROWNING*, N. M. ROBERTS and A. J. ILLINGWORTH
Joint Centre for Mesoscale Meteorology, University of Reading, UK

(Received 3 July 1996; revised 16 December 1996)

SUMMARY

The archetypal mesoscale structure of an ana-cold front comprises a narrow cold-frontal rainband (NCFR), associated with line convection, embedded within a wide cold-frontal rainband (WCFR) due to the slantwise ascent associated with a strong transverse-front mesoscale circulation. Whereas most mesoscale observational studies have concentrated on this mature stage, the present paper explores by means of a detailed case-study how such a mature frontal system develops from pre-existing features. The study is based upon the synthesis of data spanning many scales, in the form of satellite imagery, observations from conventional and multi-parameter Doppler radar, and surface reports, together with diagnostics from an operational mesoscale forecast model. The cold-frontal zone in this case is characterized by multiple cold fronts. The dominant second cold front is studied in detail from the point of view of its evolution and its relationship to neighbouring fronts, especially the leading front associated with the initial polar-front cloud band. The dominant cold front started as a shallow 'rope cloud' in the cold sector, and at a fairly early stage it produced a NCFR due to line convection. Then, over a period of only a few hours, a dry intrusion and an associated strong direct transverse-front circulation led to the formation of a canopy of mid-level cloud and a WCFR. The WCFR was attributable not only to the rearward-ascending outflow from the line convection but also to the re-invigoration of ascent within the initial polar-front cloud band that the line convection was undercutting. Although the transverse circulation was probably intensified by precipitation processes, it is inferred that it was mainly a manifestation of the larger-scale environmental flow that existed independently of the major precipitation features.

KEYWORDS: Frontal circulation Line convection Rainbands Satellite image interpretation

1. INTRODUCTION

Figure 1 is an adaptation of the frontal-fracture stage of Shapiro and Keyser's (1990) model of a developing cyclone to represent a typical frontal cyclone affecting north-west Europe. It shows the frontal analysis in relation to system-relative flows, and cloud and precipitation features as described in the caption. The figure shows four cold-frontal regions (the fronts being defined in terms of wet-bulb potential temperature, θ_w): two of these regions, i.e. along 'ab' and the cold frontal part of 'cd', are sharp cold fronts, often characterized by line convection. The region between 'b' and 'c' corresponds to a diffuse surface frontal zone. The fourth region, between 'b' and 'd', corresponds to an upper cold (θ_w) front. The studies of north-west European cyclones summarized by Browning (1997) have clarified the relationship of these fronts to the patterns of airflow, cloud and precipitation. What is less clear is the detailed manner in which the cold fronts evolve in getting to the stage depicted in Fig. 1. The broad-scale evolution in the frontal structure described by Shapiro and Keyser is evident, but the mesoscale evolution of the fronts and, in particular, the patterns of cloud and precipitation are not. The observational and mesoscale-model based diagnostic study in the present paper addresses these issues.

Our objective, to describe the evolution of the cold-frontal cloud and precipitation structure, might seem a fairly simple one; however, in practice such frontal regions tend to be complicated by multiple structure upstream in the approaching cold air, and it is not always easy to keep track of individual components of the resulting substructure. It is perhaps because of this that studies of frontal evolution often rely more heavily on model simulations than on observations. Here we shall rely on the observations rather more than on the model, although both are indispensible. Some insight into the nature of

* Corresponding author: Joint Centre for Mesoscale Meteorology, Department of Meteorology, University of Reading, Whiteknights Road, PO Box 243, Reading, Berkshire RG6 6BB, UK. (The Joint Centre for Mesoscale Meteorology is supported by the Meteorological Office and the Natural Environment Research Council through the Department of Meteorology, University of Reading.)

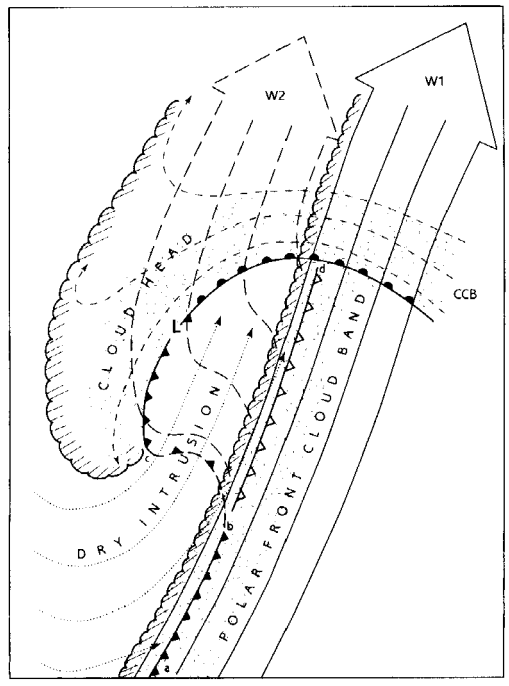

Figure 1. Structure of a developing extratropical cyclone (from Browning 1997). The cyclone centre (L) is travelling towards the top right. The surface warm front is shown conventionally. The bent-back extension of this front is plotted as a cold front with closely-spaced frontal symbols. The main surface cold front (ab) is shown similarly. In between the two sharp surface cold fronts (bc) there is a diffuse surface cold front drawn dashed with widely-spaced frontal symbols. The cold front drawn with open symbols (bd) is an upper cold wet-bulb potential-temperature front, marking the leading edge of the dry intrusion. Principal airflows, drawn relative to the system, are: the main warm conveyor belt (W1) (solid lines), the secondary warm conveyor belt (W2) (long-dash lines), the cold conveyor belt (CCB) (short-dash lines) and the dry intrusion (dotted lines). The cold-air sides of the main cloud features are drawn scalloped: the polar-front cloud band is due to W1, and the cloud head is due to the combined effect of W2 and the CCB. Precipitation (stippled shading) reaches the surface along the left side of W1, near the cold fronts, and above the warm-frontal zone; precipitation also falls from the inner parts of the cloud head, starting at the bent-back front. The two main areas of precipitation are separated by a dry slot where the shallow W2 flow is capped by the dry intrusion. The dry slot is usually characterized by partial shallow cloudiness.

the multiple structure has already been gained from the intensive observing period, IOP3, of the FRONTS 92 experiment in which a dense array of dropwindsondes was released over the Atlantic during the early stages of cyclogenesis. An analysis of the IOP3 fronts revealed two levels of fine structure (Browning *et al.* 1995): there were two distinct cold fronts about 100 to 200 km apart plus some secondary structure on a smaller scale. The primary fronts were associated with two distinct regions of dry, low-θ_w air ('dry intrusions'). These dry intrusions descended from the upper troposphere and were trackable in satellite water-vapour imagery as 'dark zones'. The two primary cold fronts appeared as surface features, producing thin lines of shallow cloud early in the process of cyclogenesis, but the subsequent evolution of individuals fronts was not well resolved on the mesoscale.

In the present case, on 24 October 1995, the cyclogenesis took place close to the British Isles, and so for much of the time when the fronts were producing precipitation, they were within range of the land-based weather radar and conventional observational networks. These, along with Meteosat imagery, revealed the development of multiple fronts which were sharp in places, one of them developing line convection ahead of a density-current-like circulation. This was confirmed by detailed Doppler measurements

from the research radar at Chilbolton (Goddard *et al.* 1994) which provided an important observational component of this study. Other parts of the fronts were shown to be less sharp, and in some places the evidence suggests they were purely upper fronts. Together with the multiple-front structure, this kind of variability, in both space and time, makes mesoscale analysis a challenging task.

The present case, in having multiple cold-frontal structure, was similar not only to the FRONTS 92 IOP3 case but also to several others we have studied superficially. We believe on the basis of these unpublished studies that such multiple (two or more) structures are very common. This would also be consistent with the multiple rainband structure that typifies the later stages of cyclone evolution (Kreitzberg and Brown (1970) and many later studies, e.g. Garratt *et al.* (1985) and Saarikivi and Puhakka (1990)). In the present study, we describe the evolution of the dominant front in particular detail while it was being activated from an initially shallow rope-like cloud eventually to become very sharp at the surface, with line convection and heavy precipitation in one part, and an upper cold front, with no surface front but still heavy precipitation, in another part. We also show that, as it intensified, this front interacted with another cold front ahead of it. For more accurate very-short-range forecasts to be made it will be necessary to understand these associated mesoscale processes and to ensure they are properly represented within numerical weather-prediction models.

The Meteorological Office's operational mesoscale model that we use as a diagnostic tool is hydrostatic, with a 17 km grid and 31 levels in the vertical, and it is nested within the 50 km grid Limited Area version of the Unified Model. It reproduced some key features of the 24 October 1995 fronts but it did not properly represent the mesoscale transverse circulation and it failed to resolve the vigour of the line convection that was embedded within it. An in-depth diagnosis of the model performance for this case will be published separately; in the present paper we make use of broad features from its output as a context for interpreting the detailed observations.

To restate the purpose of this paper, it is to study the evolution of a dominant cold front that approached from the cold sector and interacted with the leading cold front associated with a polar-front cloud band. Such interaction is a common occurrence, the particular case analysed in this paper having been selected simply because of the availability of data that reveals key aspects of the evolution. The case is complicated by the existence of more cold fronts than the two just mentioned. This, too, is a common occurrence, although usually not to the extent observed in this case. We begin with a brief synoptic overview in section 2, and this is followed in section 3 by a detailed mesoscale analysis of the evolution of the frontal cloud and precipitation as seen in satellite and radar imagery. The dynamical and thermodynamic structure of these fronts is then analysed on the basis of surface observations, output from the mesoscale model (section 4) and observations from the advanced research radar at Chilbolton (section 5). An overall synthesis is given in section 6.

2. Synoptic-scale overview

The synoptic setting for the present case-study is summarized in Fig. 2. The model used in the rest of this study is the mesoscale version of the Meteorological Office Unified Model but, first, to provide the large-scale context we use the 50 km resolution Limited Area (LAM) version of the same model. Shown in Fig. 2 is the mean-sea-level (m.s.l.) pressure analysis from the LAM superimposed upon the Meteosat infrared imagery at 6-hour intervals starting at 06 UTC 24 October 1995. The initial time shown (Fig. 2(a)) is early in the development of the cyclone of interest which formed a closed circulation several

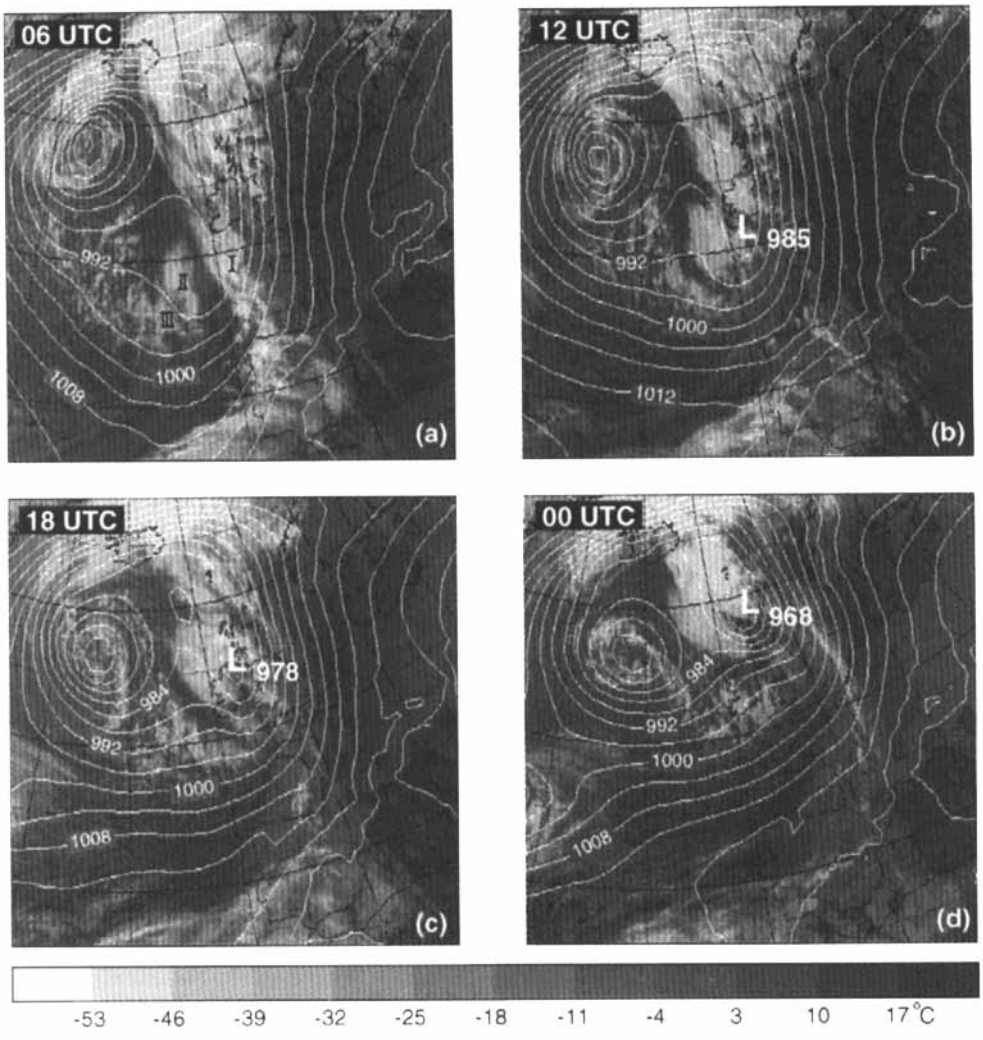

Figure 2. Synoptic overview of the case studied in this paper, from a combination of Meteosat infrared imagery and analyses from the operational Meteorological Office Limited Area Model at (a) 06, (b) 12, and (c) 18 UTC 24 October and (d) 00 UTC 25 October 1995. Lines are mean-sea-level isobars at 4 mb intervals. Cloud areas I, II and III are marked in (a); these merged into a single cloud head just south-west of the low centre 'L' by 12 UTC (b). Each of the cloud areas was associated with its own shallow cloud line extending to the south of it (more clearly evident in Figs. 3 and 4). The grey scale is linear between −53 °C (palest grey) and +17 °C (darkest grey).

hours later over Ireland. The model-derived m.s.l. pressure at 06 UTC in the area of the incipient cyclone was 991 mb, dropping to 985 mb by 12 UTC (Fig. 2(b)). Observed central pressures decreased from 984 mb at 13 UTC when the closed surface low was first observed to 974 mb at 19 UTC as the new centre travelled northwards at about 100 km h^{-1} from a location 200 km south of Ireland to the north coast of Ireland. By 00 UTC 25 October it had reached the Hebrides with a central pressure of 965 mb (968 mb in the model, Fig. 2(d)).

The dominant cloud features in Fig. 2(a) are the swirl of cloud associated with the primary cyclone near 25°W, 58°N and a long polar-front cloud band (PFCB) associated with a cold front, referred to as cold front I (CF I), which at 06 UTC was extending from west of Portugal across western Ireland to Iceland. The cloud features that formed in association

with the secondary cyclone (L) analysed in this paper can be seen developing to the west of the PFCB initially as two mesoscale cloud areas, labelled II and III (Fig. 2(a)). As they developed, II and III merged and acquired a more sharply defined cloud structure corresponding to the feature 'C' in Figs. 5.2.11–13 of Bader *et al.* (1995). This is the developing cloud head described by Browning and Roberts (1994), Bader *et al.* (1995) and others. As is clear from the full-resolution imagery (shown later), cloud features II and III occurred at the northern end of shallow and often rope-like cloud lines. Continuity with later measurements suggests that these corresponded to surface cold fronts. The case-study deals mainly with the evolution of the cold front (CF II) connected with cloud area II, and with cold front I. At the time corresponding to Fig. 2(a), there was little interaction between CF II and the PFCB associated with the initial cold front (CF I). During the next 12 hours, however, CF II merged with the PFCB, and CF I itself frontolysed, at least at low levels. The interaction of CF II with CF I conformed to the instant occlusion process as described by Zillman and Price (1972), McGinnigle *et al.* (1988) and Bader *et al.* (1995)—see, in particular, McGinnigle *et al.*'s model in their Fig. 14. The existence of further cold fronts behind CF II, as shown in section 3(a), adds complexity but does not fundamentally alter the instant occlusion process as described by those authors.

3. Mesoscale analysis of the satellite and radar imagery

(*a*) *Overview of the multiple cold-frontal structure*

Figure 3 shows a frontal analysis for 15 UTC, based on imagery, some surface observations and model output, to provide a context for the detailed meso-analyses presented in this section. The fronts are drawn along the axes of shallow cloud lines using a combined analysis of sequences of infrared and visible images. Time continuity is an important part of the analysis since single images can be ambiguous. The cloud lines show as pale grey in the infrared, punctuated by brighter (deeper) convective cloud cells along their northern parts. The shallow cloud lines often appear bright and are more obvious in the visible channel. The lines are spaced typically 100 km apart and they formed in a baroclinic region where according to the model there was negative equivalent potential vorticity. Thus conditional symmetric instability may have been involved in their formation, although large parts of the region were also potentially unstable so that upright convection is likely to have occurred more readily than slantwise convection (Bennetts and Hoskins 1979; Moore and Lambert 1993). An extended study of the mesoscale model data to be published separately will examine this question more fully.

The 15 UTC analysis time depicted in Fig. 3 is just before the onset of the mature phase of what became the dominant cold front (CF II). Several other cold fronts not discussed here in detail are shown behind it. Two of these were evanescent; the others, CF III and IV, were rather longer-lived. (CF III is analysed in JCMM Internal Report 58, available from the authors.) Ahead of the main cold front (II), CF I had already undergone frontolysis; this, along with CF II, will be discussed in section 3(b). CF I had earlier been responsible for the original PFCB ahead of the developing cloud heads II and III (Fig. 2(a)) which combined to form the single cloud head over and to the west of Ireland shown in Fig. 3. Early in their development, and throughout their development in places close to the cold fronts, the cloud heads were characterized by convective cloud but, as they grew and matured, the cloud heads became increasingly composed of stratiform cloud.

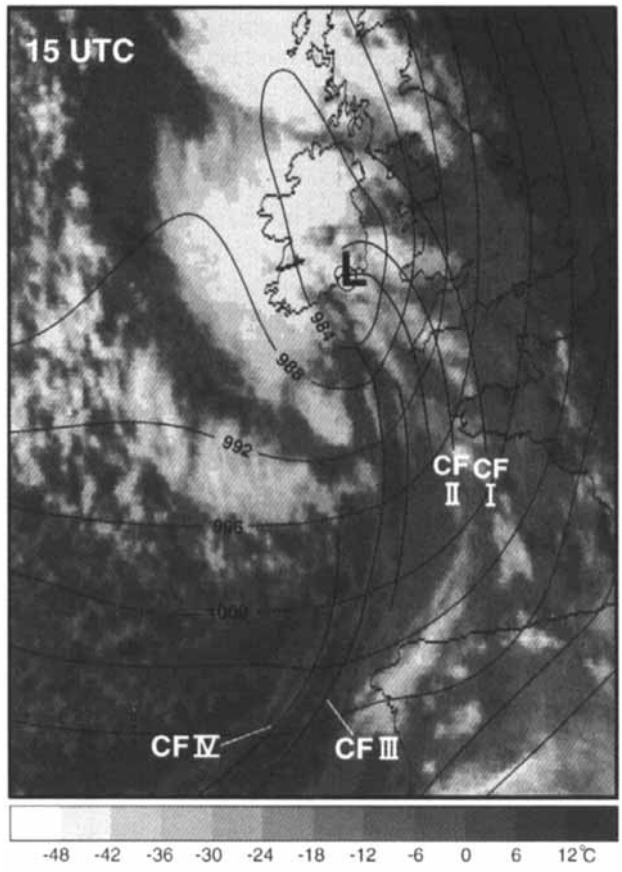

Figure 3. Analysis for 15 UTC 24 October 1995 showing multiple cold fronts (thin lines) and mean-sea-level pressure (at 4 mb intervals). The main cold fronts are labelled I, II, III and IV. Front I is the original polar front which by this time had frontolysed. The two unlabelled fronts shown between II and III were evanescent features. Meteosat infrared imagery is shown as a background; the grey scale is linear between −48 °C (palest grey) and +12 °C (darkest grey).

(*b*) *Evolution of cloud and precipitation associated with cold fronts I and II*

(i) *The early stage of CF II (< 12 UTC).* In the early stages of CF II, between 07 and 12 UTC, it was well-observed over the sea by Meteosat. It appeared as a rope cloud (e.g. Figs. 12.20d, 13.7a, 13.14 and 13.21a in Scorer 1986, and Fig. 4.1.17(a) in Bader *et al.* 1995), particularly distinctive in the visible imagery (Fig. 4(a)). We have no *in situ* measurements over the sea in the present study; however, detailed *in situ* measurements during the passage of similar rope clouds reported in the literature show that they are associated with cold fronts with abrupt wind shifts, temperature drops and pressure jumps concentrated within a strip of order 1 km wide. Observations of rope clouds in Australia (Smith *et al.* 1995) show that typically such fronts are shallow (~ 1 km deep) and dry (i.e. non-precipitating). Observations in the USA (Shapiro *et al.* 1985; Shapiro and Keyser 1990) show that, although they may be dry and shallow, vertical velocities of up to 5 m s^{-1} can nevertheless occur. Infrared imagery (Fig. 4(b)) shows that the cloud tops in the present case were between +5 and 0 °C, corresponding to a height of only 2 to 3 km. A series of tracings of the rope axis and other associated cloud features during this period is shown in the left-hand half of Fig. 5. The more complete 09 UTC tracing in Fig. 5 shows that the rope

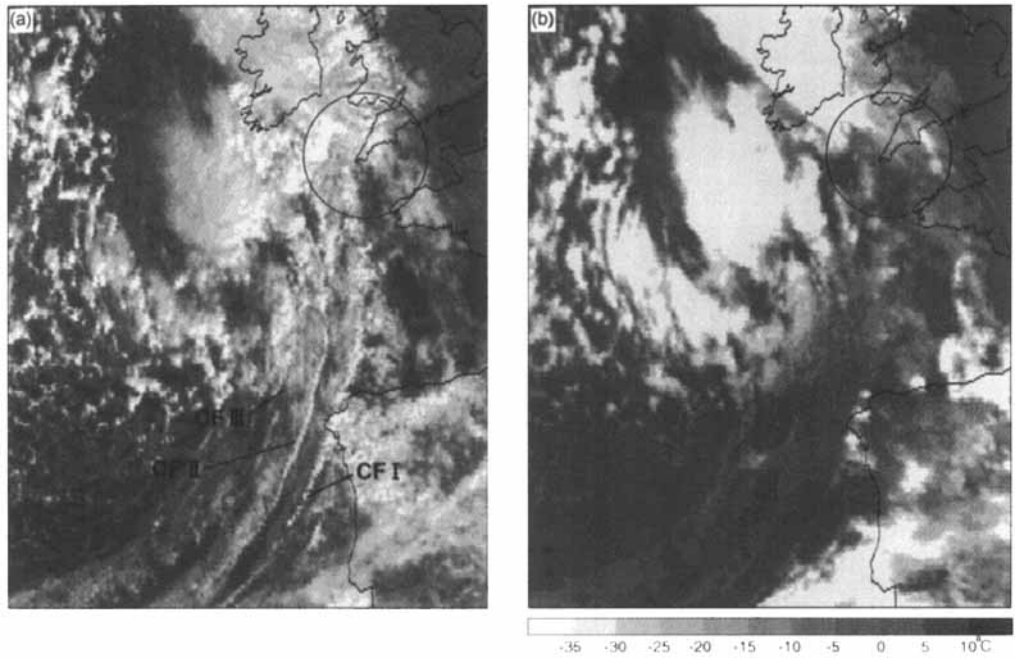

Figure 4. (a) Visible and (b) infrared Meteosat images at 1100 UTC 24 October 1995, showing cloud lines associated with cold fronts I, II and III trailing southwards from cloud heads over and to the south-west of Ireland. The grey scale in (b) is linear between −35 °C (palest grey) and +10 °C (darkest grey). The cold-frontal cloud lines show up brightly in the visible image but are harder to discern in the infrared because of their shallowness (black lines have not been superimposed as in Fig. 3 for fear of obscuring details of the image). Circles show coverage of the Cornwall radar for reference to later figures.

cloud at its northern end extended into the developing cloud head. Quantitative evaluation of the infrared imagery shows that cloud-top temperatures within the cloud head were as low as −40 to −50 °C.

Individual plumes of cold cloud, with tops estimated from the imagery to have been intermediate in height between those of the rope and cloud heads, appeared to originate from sources along the rope cloud; Fig. 5 shows these streaming away towards the north, rearwards at an angle of 30° to the rope cloud. The tops of these cloud plumes in some cases rose with distance downwind of their sources rather than having a maximum height at the source. This suggests that the plumes may have been due to boundary-layer air rising slantwise as laminae of ana-cold frontal ascent as described by Browning (1995), rather than as anvil plumes emanating from the tops of convective cells along the cold front.

(ii) *Transition of CF II towards its mature stage and its interaction with CF I (12–17 UTC).* At 12 UTC upper cloud associated with CF I, which after a period of frontolysis had just started to rejuvenate, began to obscure the CF II rope cloud as it caught up with CF I. However, it was at about this stage that the northern end of CF II came within clear view of the land-based radars, and the corresponding radar-derived frontal positions are shown in the right-hand part of Fig. 5 (and in the inset to Fig. 5). We now examine the precipitation and cloud structure as CF II came within view of the Cornwall weather radar in south-west England (Fig. 6).

Figures 6(a), (b) and (c) show the NCFR associated with CF II approaching south-west England. It can be seen to have been embedded within an extensive and rapidly

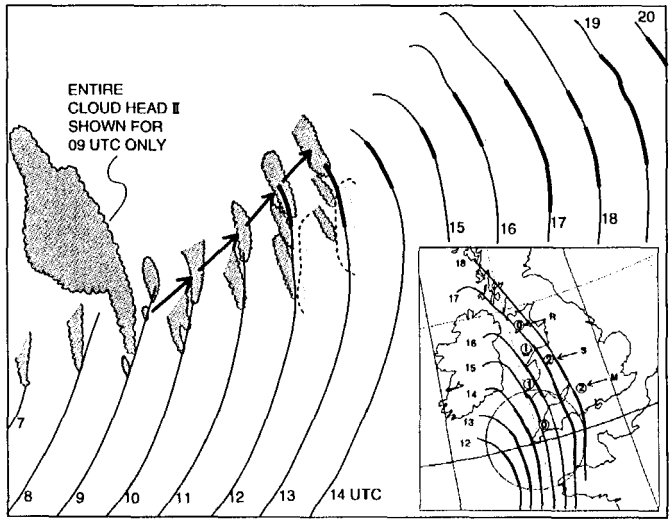

Figure 5. Hourly positions of cold front II deduced from Meteosat and radar imagery from 07 to 20 UTC 24 October 1995. Bold portions of the lines indicate regions of line convection inferred by radar. Successive frontal positions are given additional constant displacements to the right in order to provide space to show cloud plumes extending rearwards from the northern end of the line—see darkly shaded areas from 07 to 13 UTC (the entire cloud-head area associated with CF II being shown for 09 UTC only). Arrows show the displacement of specific cloud elements. The lightly shaded region bounded by dashed lines denotes the western edge of an area of higher cloud due to CF I which increasingly obliterated cloud due to CF II after 13 UTC. The inset shows frontal positions without additional displacements in order to clarify the movement of CF II in an earth-relative frame of reference. Also shown in the inset are pressure kicks (plotted in mb within the small circles) for six stations during the passage of CF II: autographic traces from three of these stations, labelled R, S and M, are shown in Fig. 14. The large circle in the inset shows the coverage of the Cornwall radar.

developing region of lighter precipitation. The NCFR evolved from a line of small cells of heavy rain at 12 UTC (Fig. 6(a)) to a thinner line of heavy rain, parts of which were sufficiently 2-dimensional to be consistent with line convection (see (b) and (c)). The corresponding Meteosat infrared pictures in Figs. 6(d), (e) and (f) show that parts of the line-convection echo for some of the time were embedded within moderately deep cloud with tops occasionally colder than −28 °C; but there was no consistent relationship between the cold clouds and the line convection and, indeed, the convection responsible for the thin line of the most intense radar echo is believed to have been much shallower. Line convection in the United Kingdom is seldom much deeper than 3 km and it was certainly no higher than this several hours later when it was within range of the vertically-scanning Chilbolton radar (section 5). However, the only observational evidence for the line convection being as shallow as this at an early stage is the fact that part of the corresponding echo (see southern part of line in Fig. 6(b) between 150 and 200 km range from the Cornwall radar) was associated with a portion of rope cloud with tops below 4.5 km (−10 °C) that could be glimpsed in the gap between areas of higher (colder) cloud (Fig. 6(e)).

Fairly regularly spaced ragged areas of upper-level (rather cold) cloud associated with CF I, identified by the small circles labelled A, B, C and D in Figs. 6(d), (e) and (f), were travelling northwards as they were undercut by CF II coming from the south-west. They can be seen getting deeper (colder) as they travelled northwards. They were also growing in horizontal extent, and were associated with the rapid increase in coverage of rain echoes surrounding the CF II line convection between 12 UTC (Fig. 6(a)) and 14 UTC

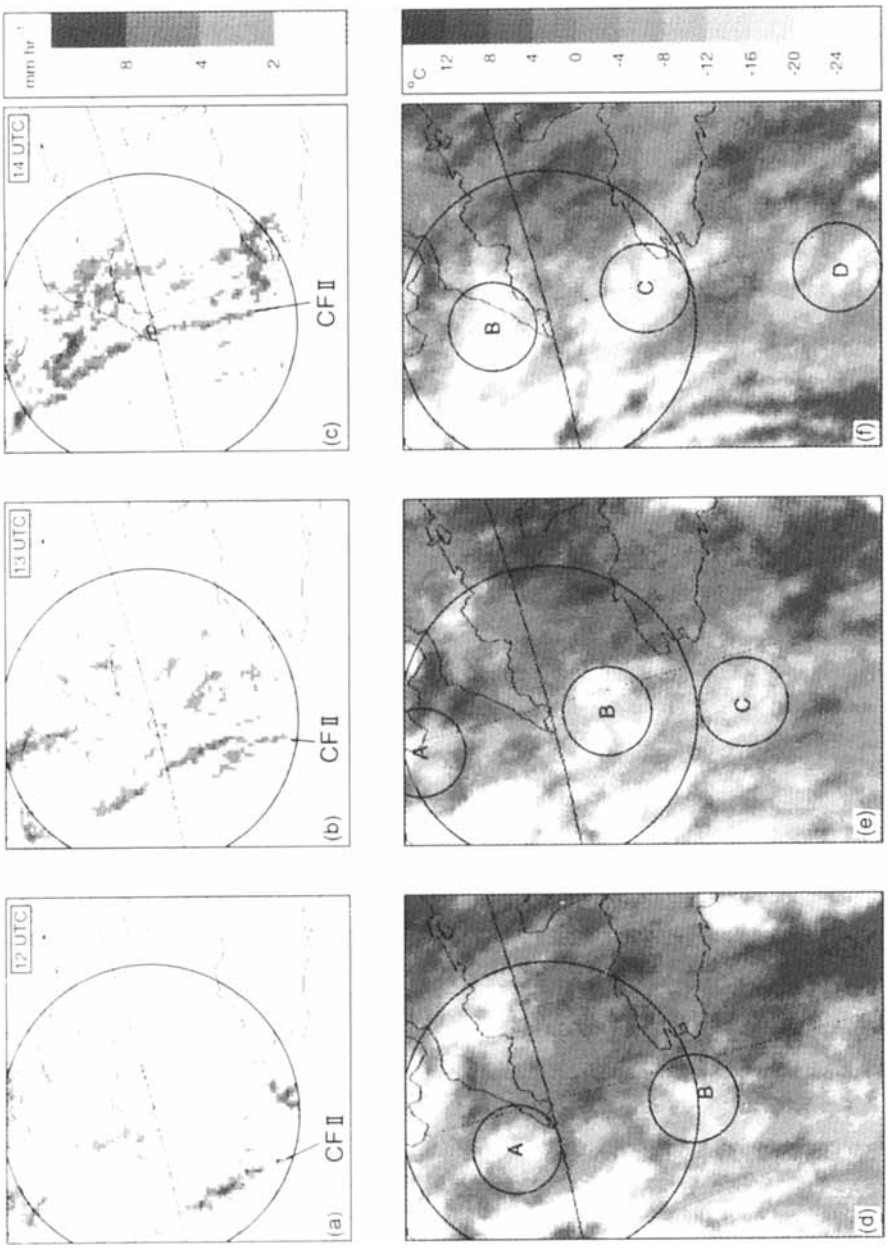

Figure 6. Radar displays ((a), (b) and (c)) and corresponding Meteosat infrared images ((d), (e) and (f)) at 12 UTC ((a) and (d)), 13 UTC ((b) and (e)) and 14 UTC ((c) and (f)) on 24 October 1995. Coverage of the Cornwall radar is shown by the large circle with radius 210 km. This is also shown on the satellite images to help in relating radar-observed features to the cloud pattern. The four grey shades in (a), (b) and (c) represent rainfall intensities < 2, 2–4, 4–8 and > 8 mm h^{-1}. The grey shades in (d), (e) and (f) represent cloud-top temperature according to a linear scale between -24 °C (palest grey) and $+12$ °C (darkest grey). The position of cold front II is indicated in (a), (b) and (c). Areas of upper cloud associated with CF I that developed into major plumes which overran CF II are identified by small circles labelled A, B, C and D.

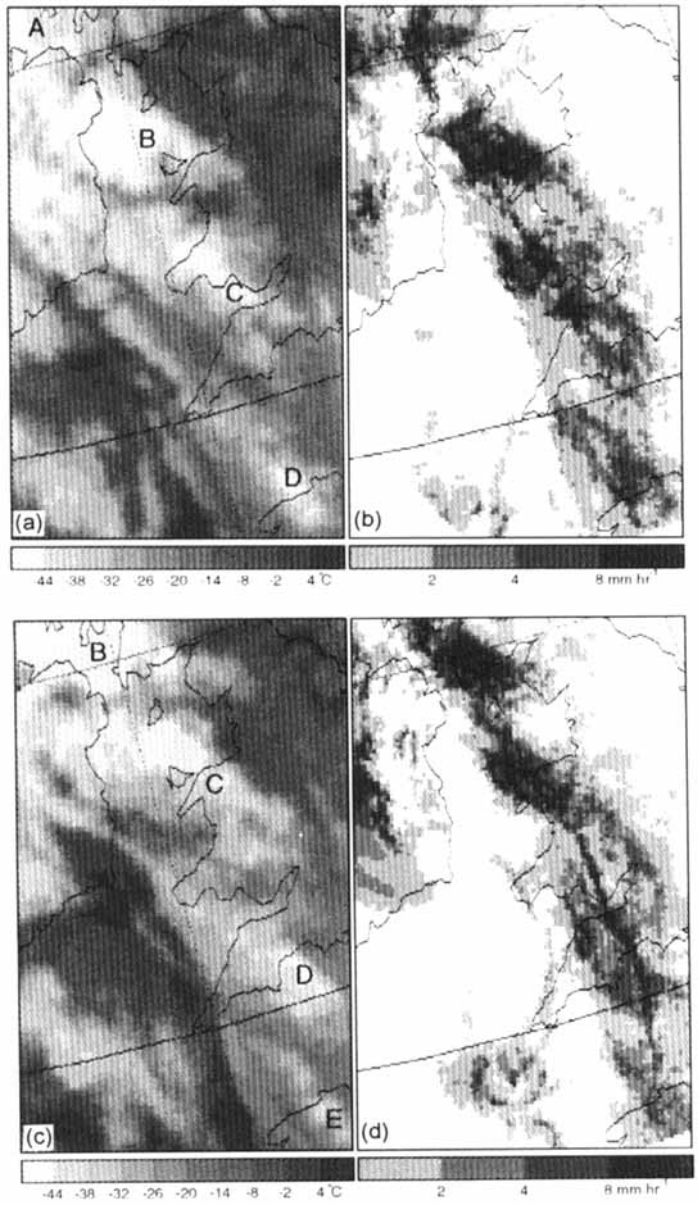

Figure 7. Meteosat infrared images and corresponding radar-network pictures, respectively, for (a) and (b) 16 UTC and (c) and (d) 17 UTC 24 October 1995. The grey shades in (a) and (c) show cloud-top temperature according to a linear scale between −44 °C (palest grey) and +4 °C (darkest grey). Cloud plumes associated with cold front I are labelled A, B, C, D and E. The four grey shades in (b) and (d) show rainfall intensities < 2, 2–4, 4–8 and > 8 mm h^{-1}.

(Fig. 6(c)). During the period to 17 UTC cloud areas A, B, C, D, and E associated with CF I continued to grow in horizontal and vertical extent (Fig. 7) to form the mesoscale plumes that so dominated the infrared imagery at the later times. Their growth during this period appeared to be occurring in association with the same belt of mesoscale ascent that was responsible for the increasing vigour of CF II which was undercutting them. By 1700 UTC CF II was producing a well defined NCFR which shows clearly in Fig. 7(d).

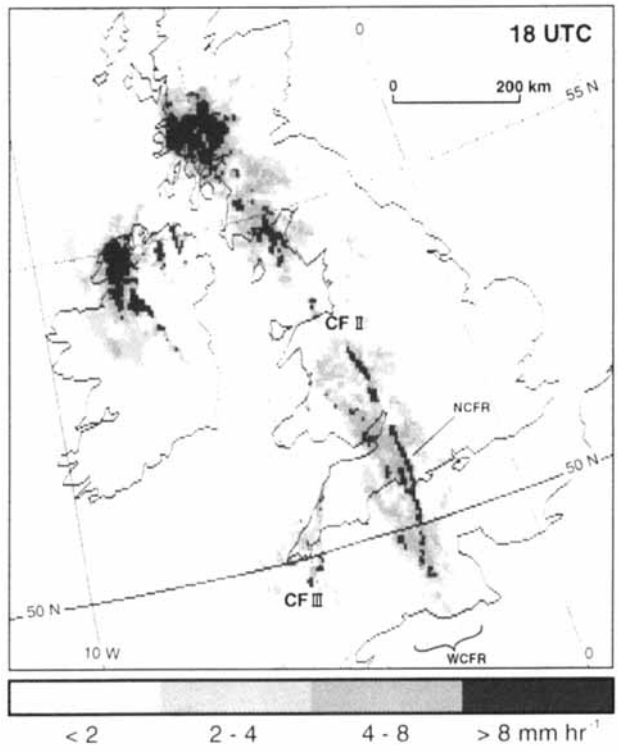

Figure 8. Radar-network picture for 18 UTC 24 October 1995. The four grey shades represent rainfall intensities of < 2, 2–4, 4–8 and > 8 mm h^{-1}. The main belt of rain extending from France to Scotland is a wide cold-frontal rainband due to cold front CF II, with a small contribution from CF I. The thin line of heavy rain embedded within it, from the English Channel to the north Wales border, is the narrow cold-frontal rainband due to CF II. The thin line of rain extending from south-west England southwards near 5°W to Brest, with a more general area of rain over extreme south-west England, is associated with CF III. A surface analysis giving the position of these fronts is shown in Fig. 13. The rain area over Ireland is associated with the main cloud head associated with CF II and CF III. A coloured version of the 1830 UTC picture is shown on the cover of AMS (1996).

(iii) *The mature stage of CF II (~18* UTC*).* By 18 UTC the radar-network picture in Fig. 8 shows that there was a narrow band of heavy rain embedded within a 150 km-wide band of increasingly uniform light-to-moderate rain. These had become, by then, archetypal examples of the narrow and wide cold-frontal rainbands in the classification of Houze *et al.* (1976). The WCFR extended from France to Scotland but the NCFR extended only between latitudes 49°N and 53°N. Data in sections 4 and 5 confirm that the latter was indeed line convection associated with a sharp surface cold front. The portions of CF II drawn boldly in Fig. 5 show the radar-derived extent of this line convection at different times. To the north of the line convection, over the Irish Sea and eastern Ireland, the positions of CF II in Fig. 5 have been inferred by radar from the locus of more scattered outbreaks of convective precipitation. Here the cold front was no longer a surface feature; rather, as shown in section 4, it was an upper cold (θ_w) front. The WCFR in Fig. 8 was the result of a rearward-ascending slantwise flow, typical of an ana-cold front. We show later (section 5) that this rearward-ascending flow was composed partly of outflow from the CF II line convection itself and partly of moist air associated with the old CF I.

(iv) *The transition from an ana- to a kata-circulation as seen in the CF I cloud pattern.* Figure 9 shows that the mesoscale cloud plumes identified in Figs. 6 and 7 developed

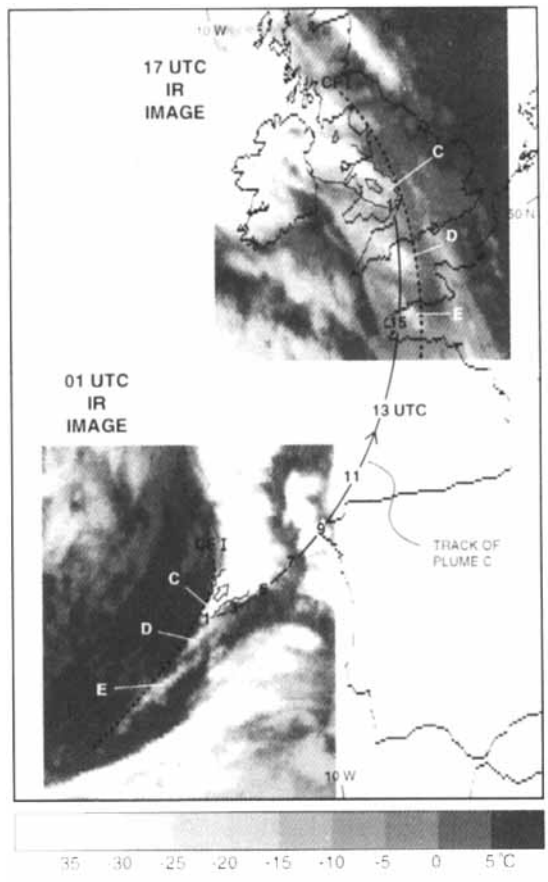

Figure 9. Successive 2-hourly positions on 24 October 1995 of cloud plume C associated with cold front CF I, anchored with respect to the infrared imagery at the beginning (01 UTC) and end (17 UTC) of the tracks. Other cloud plumes (e.g. D and E) could be followed along almost parallel tracks. CF I is shown by the dashed lines through the upwind ends of the plumes at 01 and 17 UTC. The grey shades represent cloud-top temperatures according to a linear scale between −35 °C (palest grey) and +5 °C (darkest grey). The 01 and 17 UTC images show the cloud plumes to be forward-trailing and rearward-trailing, respectively, and a cloud outline and arrow is marked in each case to emphasize this for cloud plume C.

from the residues of previous strongly convective areas of cloud that could be traced from 01 UTC (and earlier) when the PFCB associated with CF I had been intense. Sferics observations showed that the cloud area that developed into plume C, for example, had been a thunderstorm within the PFCB at 01 UTC. At this time it was producing a forward-trailing anvil and was located at $41\frac{1}{2}°$N 14°W. The *forward*-trailing behaviour of this anvil, and the other similar anvils, is consistent with an overrunning kata-cold frontal circulation characterizing CF I as it underwent frontolysis. By 09 UTC storm areas C, D and E, along with their neighbours along the PFCB, had almost entirely decayed. But then, from 11 UTC onwards, as shown by Figs. 6 and 7, these areas of cloud, and others like them along the old frontolysed CF I, began to develop into the mesoscale plumes which this time were trailing *rearwards* in association with what was evidently a newly developing ana-cold frontal (i.e. direct) circulation. These rearward-trailing plumes were shallow at first with tops below 5 km but, as the ana-circulation became established, they steadily deepened to about 9 km corresponding to a cloud-top temperature of −45 °C (Fig. 7).

We interpret the plumes A–E as being due to air, moistened by the evaporation of the anvil residues from earlier convection along CF I, coming under the influence of a band of renewed synoptically forced ascent which was invigorating both them and the CF II line convection. Our purpose is to describe the evolving response of small-scale cloud and precipitation events to changing larger-scale forcing; it is beyond the scope of the paper to diagnose the cause of the change from kata- to ana-circulation in this region other than to say that its onset preceded, and was presumably independent of, the generation of mesoscale rearward-sloping outflow from the line convection, discussed next.

(v) *The contributions of CF I and CF II to the wide cold-frontal rainband (1600–1830* UTC*).* Figure 7(c) shows that at 17 UTC the upper-level plumes due to CF I were superimposed upon a wide band of middle-level cloud, with background tops at about 5 km (−15 °C) (medium grey), that was by then completely enveloping the CF II line convection and was due in large measure to it (cf. section 5). (This is much clearer when the imagery is viewed in false colour; see AMS 1996.) One to two hours later, at the time of the Doppler radar measurements in section 5, the tops of this background cloud canopy had risen to 5.5 km whilst the tops of the mesoscale plumes remained at 8 km (over southern England). Evidence in section 5 shows that the CF I plumes were situated just above the region of cloudy slantwise ascent that was being generated by the outflow from the CF II line convection. The demarcation between cloud due to CF I and that due to CF II cannot be determined precisely, but the later analysis suggests that from 18 to 19 UTC it occurred between 5 and 7 km. By 1830 UTC the WCFR had become fairly 2-dimensional. However, before this, the WCFR had been distinctly non-2-dimensional and, indeed, at 16 and 17 UTC Fig. 7 shows that the pattern of rainfall within the WCFR bore the clear imprint of the CF I cloud plumes shown by Meteosat. Evidently, therefore, the rainfall in the WCFR at this time was being strongly influenced by CF I. The more nearly uniform pattern of rainfall at 18 UTC (Fig. 8) and especially at 1830 UTC (AMS 1996) shows that the WCFR eventually became dominated by the more nearly 2-dimensional rearward-sloping outflow from the CF II line convection.

4. Mesoscale analyses of the dynamic and thermodynamic structure of the cold fronts

(*a*) *Mesoscale model analyses*

Figure 10 shows model-derived analyses for 18 UTC, at a time when the model would have been benefiting from land-based surface and upper-air observations representing the detailed frontal structure. The figure shows θ_w analyses at 850 mb (Fig. 10(a)) and 650 mb (Fig. 10(b)) and the corresponding relative-humidity analyses at these two levels (Fig. 10(c) and Fig. 10(d)). Also marked are an upper cold front and two sharp surface fronts produced by frontal fracture as in Fig. 1. One of the sharp surface fronts in Fig. 10 is an almost stationary warm front extending down the west coast of Scotland to the centre of the surface low (L) and terminating as a bent-back front near south-east Ireland. The other front, extending from Britanny northwards to south-west Scotland, corresponds to CF II. This is analysed on the basis of the radar and surface data (see later) as a sharp surface feature (solid cold-front symbols) over much of its length but as an upper feature only (open symbols) north of the point where it crosses into the Irish Sea. This is seen to be consistent with the model-derived θ_w pattern which shows the front to be situated at the leading edge of the θ_w gradient all along its length at 650 mb (Fig. 10(b)) whereas at 850 mb the leading edge of the θ_w gradient appears to be holding back along the north Wales coast (X in Fig. 10(a)) reminiscent of the schematic in Fig. 1. The other cold fronts

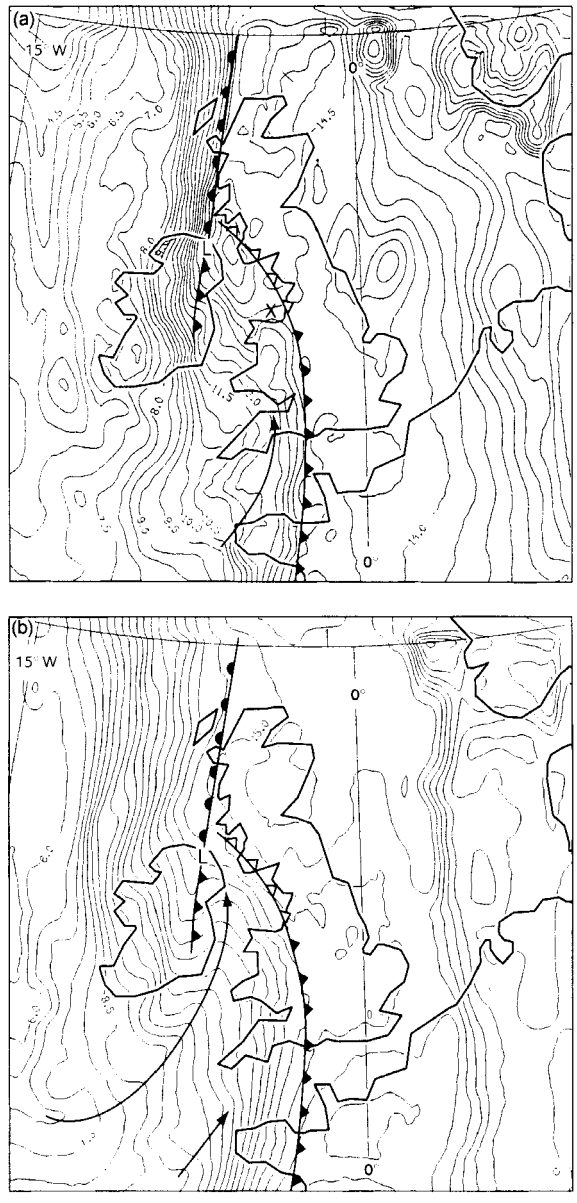

Figure 10. Mesoscale model-derived analysis for 18 UTC 24 October 1995, showing (a) and (b) wet-bulb potential temperature, θ_w, and (c) and (d) relative humidity at (a) and (c) 850 mb and (b) and (d) 650 mb. Contours of θ_w are plotted at 0.5 degC intervals. Relative humidity is plotted at intervals of 5% (shaded in excess of 90%). Analysed fronts are based on the model-derived θ_w fields; their positions differ slightly from the observed positions in Fig. 13. The arrows denote axes of two fingers of dry-intrusion air referred to in the text. The southern finger is apparent at both 850 and 650 mb but the northern finger is apparent only at the higher level ((b) and (d)). The letter X in (a) marks the position near the north Wales coast referred to in the text. The dashed line AB in (c) shows the location of the 950 km-long cross-sections in Fig. 12 (the radar sections in Fig. 15 occupy part of this line).

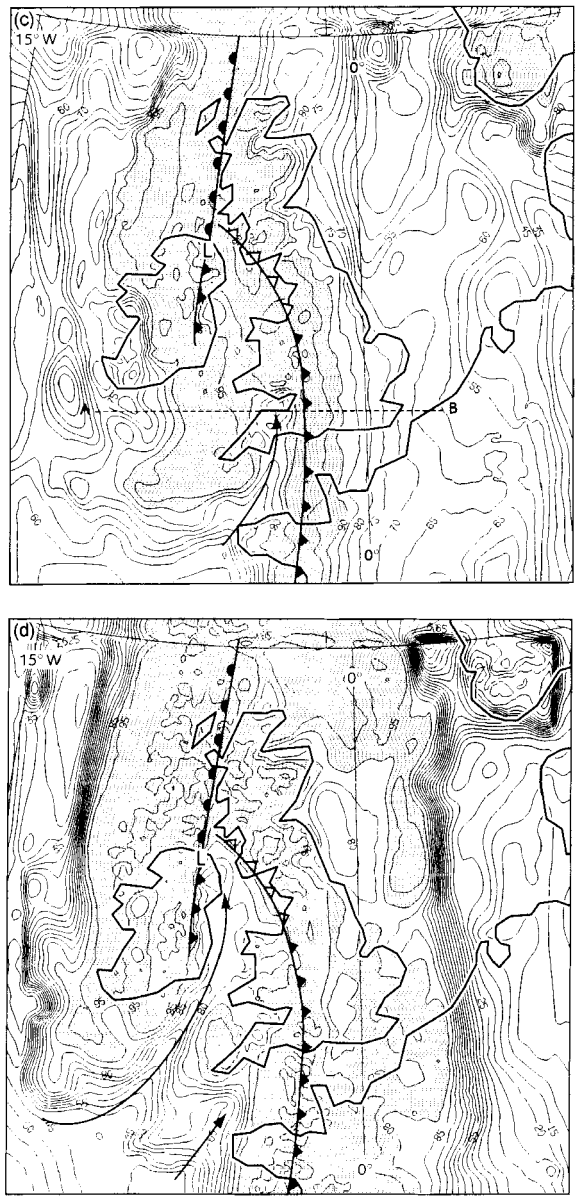

Figure 10. Continued.

diagnosed in section 3 are not marked on Fig. 10: CF I had frontoloysed by this time, at least at the surface, whilst CF III and CF IV, still further behind, may have been associated with the (ill-defined) regions of tightened gradient close to the 11.5 and 8.5 °C contours in Fig. 10(a).

The dry air shown in Figs. 10(c) and (d) digging in behind CF II is regarded as a key feature in the analysis. This is the 'dry intrusion'. Appropriate vertical sections (not illustrated) show that in the region of the Irish Sea, behind the CF II upper cold front and just ahead of the bent-back front, the dry-intrusion air at 650 mb (see long arrow in Fig. 10(d))

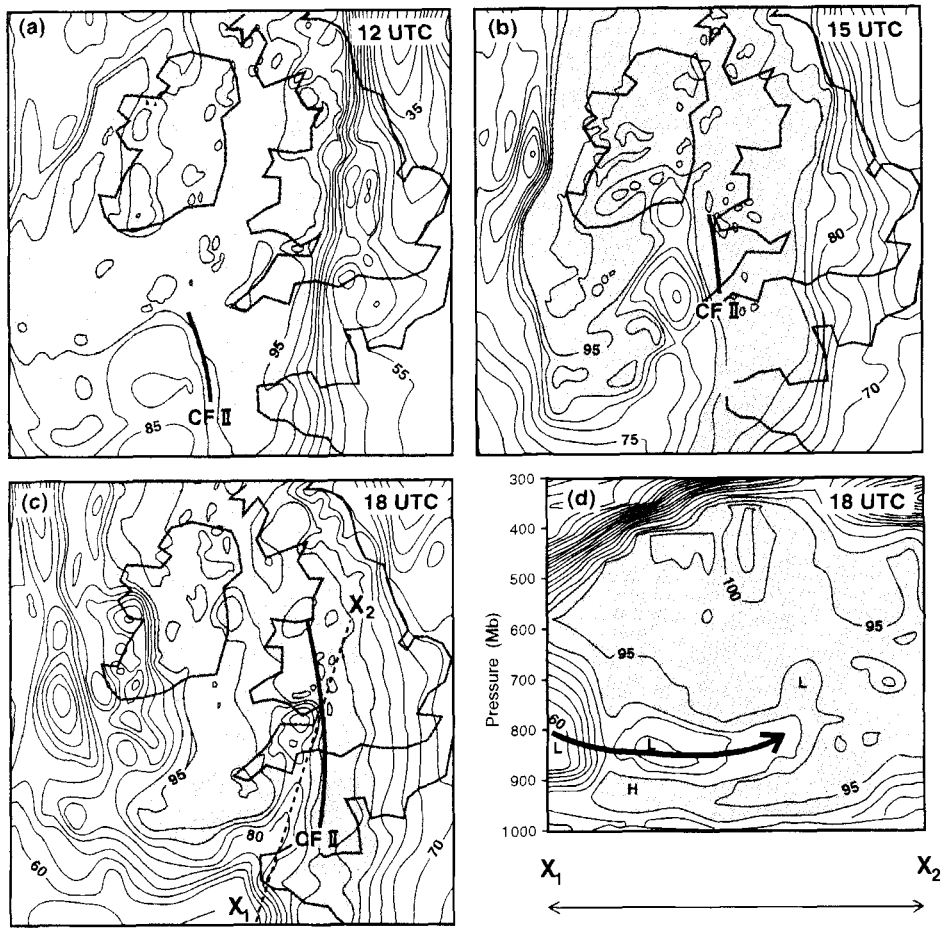

Figure 11. (a), (b) and (c) Plan sections at 850 mb and (d) cross-section showing relative humidity (at 5% intervals, shaded >90%) as derived from the 12 UTC and 18 UTC forecast runs of the mesoscale model on 24 October 1995. (a) 12 UTC, (b) 15 UTC, and (c) and (d) 18 UTC. Positions of cold front II where it is a sharp feature, as inferred from radar, are plotted in (a), (b) and (c). The section in (d) is orientated along the axis of the dry intrusion (along the 720 km-long line X_1X_2 in (c)).

was overrunning a moist zone within which relatively warm moist air (corresponding to the W2 flow in Fig. 1) extended from the surface up to about 750 mb. Farther south, a finger of dry-intrusion air can be seen at 650 mb and at the 850 mb level (see arrow in Fig. 10(c)) extending northwards across south-west England just behind the surface frontal position of CF II. A vertical section along the 850 mb axis of this finger, plotted in Fig. 11(d), shows it entering at low levels from south-west of Britanny. The sequence of 850 mb diagrams in Fig. 11 for 12, 15 and 18 UTC, derived from the 12 UTC (T+0, T+3) and 18 UTC (T+0) model runs, shows a consistently close relationship between the leading edge of the dry-intrusion finger and the sharp surface cold front as CF II developed from 12 to 18 UTC. Observational evidence presented later shows that the dry-intrusion finger was the forward-directed part of a strong mesoscale circulation transverse to the cold front. We shall be arguing that this dry-intrusion finger played a role in driving the line convection that was occurring along CF II.

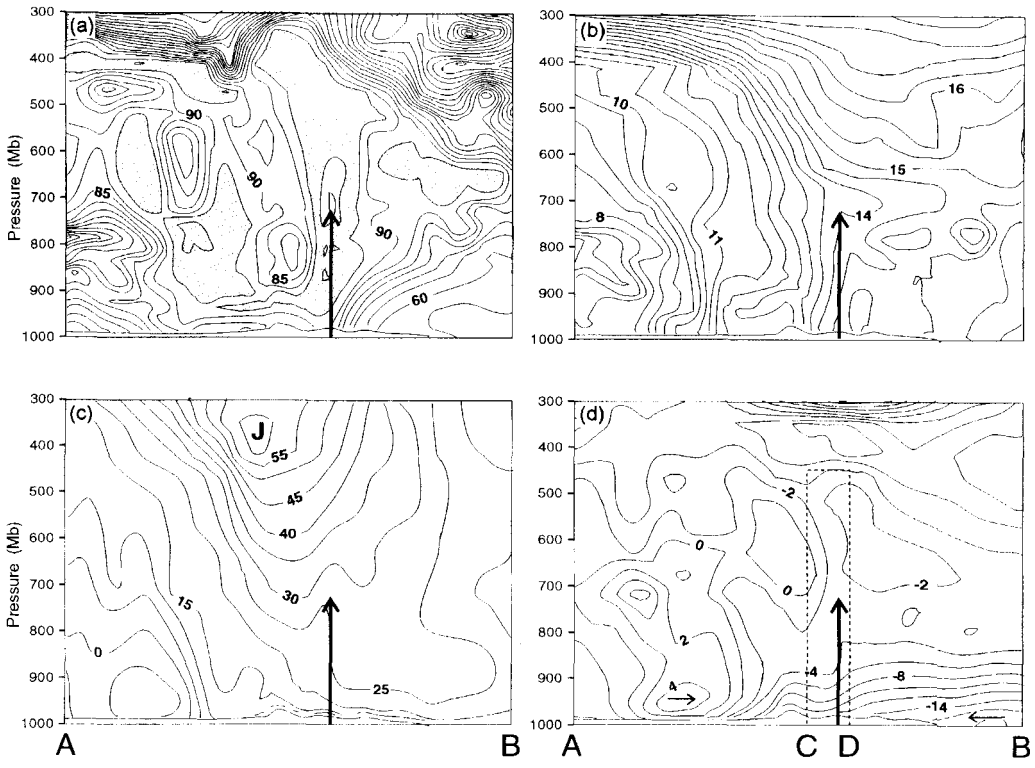

Figure 12. Cross-sections at right angles to cold front II (along the 950 km-long line AB in Fig. 10(c)) showing (a) relative humidity (contours at 5% intervals, shaded >95%), (b) wet-bulb potential temperature (contours every 0.5 degC), (c) front-parallel wind component (contours every 5 m s^{-1}) and (d) front-normal relative wind component (contours every 2 m s^{-1}), as derived from the mesoscale model-derived analysis at 18 UTC 24 October 1995. The vertical arrow extending up to almost 700 mb represents the observed position of line convection at cold front II. The dashed frame within (d) shows the 90 km-wide region covered by the Doppler radar cross-section in Fig. 15(a).

Further insight into the nature of this dry finger is provided by the west–east section across it in Fig. 12 obtained from the model-derived analysis for 18 UTC. The relative-humidity pattern in Fig. 12(a) shows that the finger of dry air was situated just behind and beneath the rearward-sloping base of the canopy of moist air (shaded region up to about 350 mb) part of which was producing the WCFR associated with CF II and the residues of CF I. The vertical arrow extending up to almost 700 mb in Figs. 12(a)–(d) represents the observationally determined position and extent of the CF II line convection. This was pumping up boundary-layer air with a model-derived θ_w of 14.5 °C (Fig. 12(b)) associated with strong pre-frontal low-level winds which exceeded 25 m s^{-1} at 850 mb (Fig. 12(c)). Later we shall show that there were much sharper changes in temperature (Fig. 14(b)) and in wind (Fig. 14(a)) across the line convection than shown by the model. The poor model performance in this regard may be attributed to factors that prevented air in the model's dry finger from penetrating to the ground and advancing as a density current behind CF II. Part of the problem lies in the weakness of the model's transverse circulation in the vicinity of CF II (Fig. 12(d)). The Doppler radar observations presented later (Fig. 15) reveal a much stronger component of relative flow approaching the front within the dry intrusion, overlain by a stronger front-to-rear flow. The more detailed study of the model performance, to be

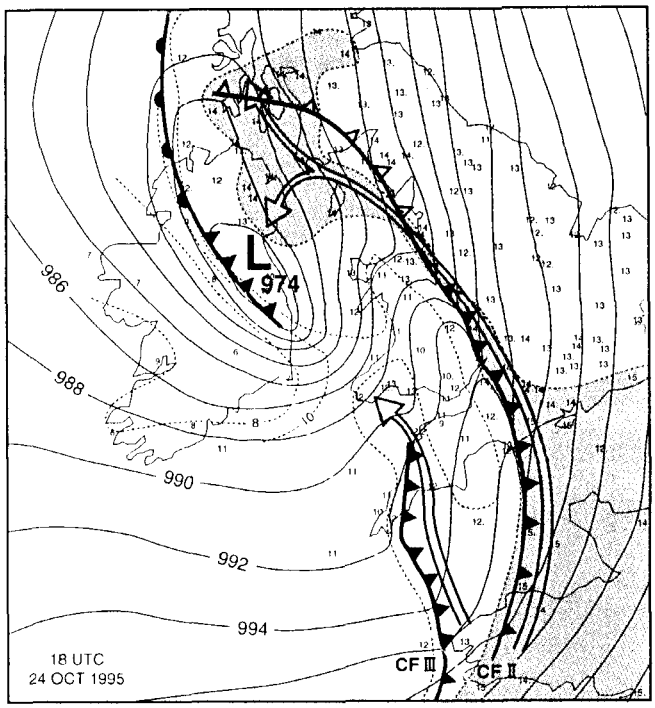

Figure 13. Detailed surface and frontal analysis for 18 UTC 24 October 1995. Thin solid lines are isobars at 2 mb intervals. Dotted lines show wet-bulb potential temperature (θ_w) at 2 degC intervals: individual station values are also plotted (a dot means $\frac{1}{2}$). Areas warmer than 12 and 14 °C, respectively, are shaded lightly and moderately, and the axes of the main warm-conveyor-belt flows are represented by long arrows. Also shown are cold fronts CF II and CF III and the bent-back front; portions of surface cold fronts with and without line convection, respectively, are marked with closely and widely spaced solid frontal symbols, and the upper cold θ_w-frontal part of CF II is marked with open frontal symbols.

published separately, reveals that other cross-sections did show rather more evidence of a transverse circulation than in Fig. 12(d), especially a few hours later.

Figure 12(a) shows another, shallower, canopy of moist air (shaded), extending up to about 650 mb just behind the dry finger discussed above. This was related to CF III which, according to Fig. 8, was generating a region of moderate stratiform rain between $4\frac{1}{2}$°W and 7°W at latitude 50°N. The canopy of moist air associated with CF III can be seen in Fig. 10(d) reaching the 650 mb level over extreme south-west England.

(*b*) *Surface observational analyses*

The m.s.l. pressure analysis for 18 UTC is shown in Fig. 13, together with a frontal analysis and a schematic portrayal of the high-θ_w surface flows (warm-conveyor-belt flows) ahead of CF II and CF III. The frontal analyses are consistent with those derived from the imagery, the model and with reports from surface stations. Over most of England the main front, CF II, produced a sharp pressure kick as shown by stations M and S in Fig. 14(a). Farther north, however, where this front is diagnosed as a purely upper cold front, station R shows no such pressure jump in association with the passage of CF II. The high-θ_w air in Fig. 13 is seen not to have penetrated behind CF II at the surface over southern and central England where the latter is analysed as a surface cold front. But, to the north of this, it flowed rearwards underneath CF II, where it is analysed as an upper cold front,

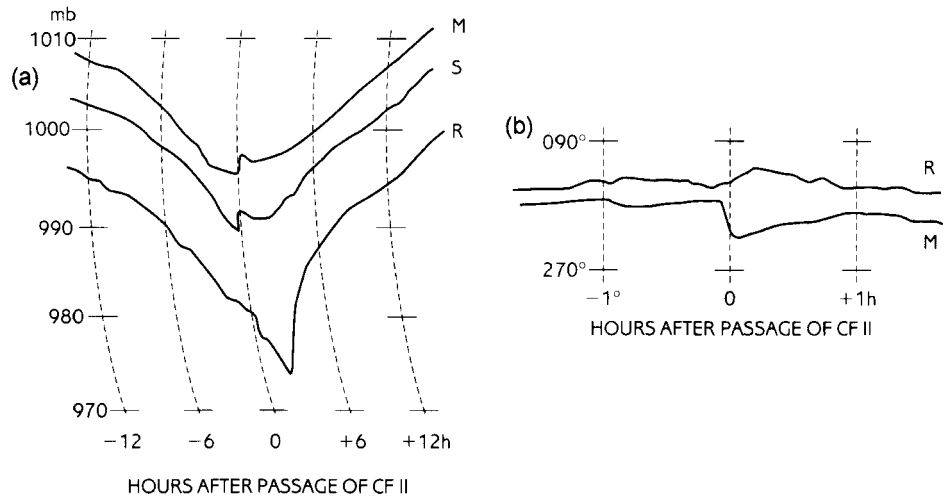

Figure 14. Tracings of autographic charts showing (a) mean-sea-level pressure and (b) wind direction during the passage of cold front CF II at approximately 18 UTC 24 October 1995 at Middle Wallop, 51°19′N, 01°34′W (station M); Shawbury, 52°48′N, 02°40′W (station S); and Ronaldsway, 54°05′N, 04°38′W (station R); the traces have been displaced so that T=0 corresponds to the passage of CF II. The locations of stations M, S and R correspond respectively to the plotted values 2, 2 and 0 near the 18 UTC position of the front in the inset to Fig. 5.

before finally ascending at the bent-back front close to the low centre. Air within the high-θ_w surface flow just ahead of the surface cold front over England also had a rearward component relative to the advancing front within the frictionally backed lowest kilometre, but this ascended as line convection at the cold front (see section 5) rather than flowing beneath it. This is consistent with the abrupt veer in the surface wind at stations such as M in Fig. 14(b) and is in contrast to the lack of a corresponding veer at the northern station R.

Just behind the CF II line convection, Fig. 13 shows a strip of lower-θ_w air (10–11 °C). It is separated from the main push of cold air behind CF III by a resurgence of (slightly) higher-θ_w air due to warm advection just ahead of CF III. This strip of lower-θ_w air is about 400 km long and 100 km wide, and is attributable to cold air brought down to the surface within a descending circulation behind CF II. The observed θ_w values of mainly 10–11 °C in this region are 1–2 degC colder than the surface values at the corresponding location as given by the mesoscale model (Fig. 12(b)). This shortcoming of the model is consistent with its underestimating the transverse frontal circulation (as confirmed in section 5).

The strip of lower-θ_w surface air just behind CF II was observed to elongate with time from 17 to 20 UTC (not shown), in accordance with the growing north–south extent of the CF II line convection during this period. This is somewhat in contrast to the model-derived evolution which, although depicting a northward displacement of the finger between 12 and 15 UTC (Figs. 11(a) and (b)), showed no more northward displacement at 18 UTC. This is a further indication of the model's failure to reproduce the correct mesoscale behaviour of the dry-intrusion finger.

5. Observations of CF II from the Chilbolton radar

The high-power multi-parameter Doppler radar at Chilbolton was being operated as part of the Hydrological Radar Experiment during the passage of the belt of rain associated with CF II. It was operated in a sequence of Range–Height Indicator (RHI) scans roughly

at right angles to the front, interspersed with Plan Position Indicator (PPI) scans over a 90° sector. We shall present data from two RHI scans to reveal the nature and true sharpness of CF II during its mature stage.

(*a*) *Transverse circulation at CF II*

Figures 15(a) and (b) show radar information obtained from an RHI scan along 268°, at right angles to the approaching cold front, CF II, at 1839 UTC: Fig. 15(a) shows almost the full width of the associated WCFR whereas Fig. 15(b) focuses on the portion close to the embedded NCFR (line convection). The colours in Fig. 15(a), giving the pattern of radial Doppler velocity, draw attention to the pronounced region of horizontal convergence below 1.5 km and divergence above 1.5 km at the location of the line convection (26 km range). Except close to the radar, in a relatively uninteresting region at upper levels, these radial velocities are a good approximation of the transverse-front velocities, from which it has been possible to derive the streamline pattern in Fig. 15(a), assuming 2-dimensional flow.

The streamlines in Fig. 15(a) show three main flows, drawn relative to the motion (left to right) of CF II:

Flow 1—This is the main precipitation-producing flow of high-θ_w air originating in the boundary layer ahead of the front. The associated streamlines (starting in the blue area on the right) show the boundary-layer air travelling from right to left and being lifted rapidly through 2 to 3 km before ascending gently aloft and contributing to the 80 km-wide region of light-to-moderate precipitation behind the surface front (the WCFR ended just beyond the 95 km range of the display). Over a zone $\frac{1}{2}$ to 1 km wide in the line convection, at a height of 1 to $2\frac{1}{2}$ km, the updraught velocities are calculated to have been over 15 m s^{-1} although this may be overestimated somewhat owing to inadequacy of the 2-dimensional assumption. Within the slantwise-ascending region of strongest (> 10 m s^{-1}) rearward flow (blue shading between the 3 and 5 km levels), the streamlines can be seen to rise 2 km over a distance of 60 km, corresponding to a mean updraught of 30 cm s^{-1}. Again, this is subject to some overestimation owing to the 2-dimensional steady-state assumption, but there was clearly an extensive region with substantial stratiform ascent.

Flow 2—This is the rear-to-front (RTF) flow of cold air that was catching up (from left to right) with CF II at low levels. The associated streamlines enter Fig. 15(a) within the red shaded layer at and just below 2 km but then they mostly turn around and ascend rearwards below 'Flow 1'. The strength of the RTF inflow puts it into the 'strong rear inflow' category as defined by Smull and Houze (1987). The fact that the RTF inflow velocity of 12.5 m s^{-1} found at the trailing edge of the WCFR (left-hand boundary of the red area in Fig. 15(a)) decreased towards the surface cold front suggests that the RTF inflow was driven more by the environmental flow than by the internal dynamics due to precipitation. Nevertheless, as suggested by Yang and Houze (1995), the microphysics and especially the evaporative cooling are likely to have been important in maintaining the observed fairly strong RTF inflow all the way to the position of the surface cold front.

Flow 3—This is the region ahead of the line convection (i.e. close to the radar), between a height of 1 and 5 km, which has a very small relative velocity component within the plane of the diagram (yellow and orange shading with few streamlines). It corresponds to the part of the warm-conveyor-belt flow above its frictionally turned 'Flow 1' portion. According to Fig. 12(c), it has a strong (> 25 m s^{-1}) parallel-front component.

In addition there was another region, Flow 4, which was more clearly evident in RHI scans for other times (not shown). This was a rearward flow similar to 'Flow 1' but situated above it at times when the mesoscale plumes associated with CF I (see section 3(b)(v))

were encountered within the Chilbolton radar cross-section. Flow 4 was characterized by a typically 2 to 5 m s^{-1} rearward component within patches of weak precipitation echo at heights between 6 and 8, and occasionally 9 km. Probably some of the flow between 5 and 6 km in Fig. 15(a) can also be attributed to Flow 4 since the limitations in the 2-dimensional assumption would most likely imply that the uppermost streamlines due to Flow 1 should be at a rather lower level than shown.

The nature of the flow in the immediate vicinity of the line convection, i.e. the surface front, is revealed more clearly by the expanded scales used in Fig. 15(b). The shading in this diagram refers to quantities discussed in section 5(b); for the moment we continue focusing on the streamlines which are depicted here at closer intervals than in Fig. 15(a). As in the cases studied by Carbone (1982), Hobbs and Persson (1982) and Parsons (1992), the flow of cold air at low levels behind the surface front (Flow 2) has some of the hallmarks of a density current. Firstly, the flow is catching up the surface front; forward relative velocities in excess of 2 m s^{-1} occur over a depth of 1 km centred at a height of 1 km. Secondly, the depth of the forward flow tends to increase within a 'head'-like region 5 km behind the surface front; the lower part of the flow descends and flows rearwards in a shallow frictionally retarded undercurrent, while the upper part rises eventually to flow parallel to the overriding Flow 1. And, thirdly, in the 'head' region there is evidence of waves or eddies of wavelength 2 or 3 km which may be due to the Kelvin–Helmholtz shearing instabilities that can be expected at the top of a density-current head.

(*b*) *Thermodynamic structure of the line convection*

We shall now consider the information shown by the shading in Fig. 15(b) and also in Fig. 15(c), which is a similar figure but for an RHI section (along a marginally different direction) 6 minutes later. The lighter shades represent radar reflectivity values in excess of 44 dBz, the threshold being set high to exclude all of the precipitation echo except for that produced by the line convection itself. The peak values of 53 dBz observed over a horizontal scale of 0.5 km correspond to rainfall intensities of roughly 100 mm h^{-1} sustained over $\frac{1}{2}$ minute during the passage of the echo core. The darker shades represent areas with linear depolarization ratios (LDRs) in excess of −24 dBz, and the purpose of depicting these is to draw attention to the height of the melting level which shows up as an LDR 'bright-band' between 2 and 3 km. In Fig. 15(b) the melting level varies in height by less than 300 m but in Fig. 15(c) there is a major variation of 900 m in the immediate vicinity of the line convection. A large proportion of the RHI cross-sections resembled Fig. 15(c). As we now demonstrate, this anomalous behaviour of the melting level enables us to make interesting inferences about the thermodynamics of the line convection.

The LDR bright-band can be taken as an indicator of the height of the 0 °C wet-bulb temperature. Knowing this height and assuming the air is saturated within the bright band, it is possible to estimate the θ_w characterizing each part of the bright band. The values of θ_w at locations 'a', 'b' and 'c' in Fig. 15(c) can be related to different parts of the flow field as follows. The lowest of these θ_w values, 11.5 °C, is situated at location 'a' (at a height of 2.2 km) just behind the line convection within the head of the density current and is indicative of the cold air just behind the front. This is consistent with surface values plotted in Fig. 13. The highest θ_w value of 14.5 °C, situated at location 'b' where the bright band reaches a height of 2.9 km, is within air that has ascended from the boundary layer ahead of the line convection (dashed streamline). Again, this is consistent with the observed surface values just ahead of CF II in southern England, plotted in Fig. 13.

At location 'c', the value of θ_w is 12.7 °C; this location is also ahead of the line convection and it is situated at a height of 2.4 km directly above the 14.5 °C air that feeds the line convection. This implies a 1.8 degC lapse in θ_w, i.e. significant low-level potential

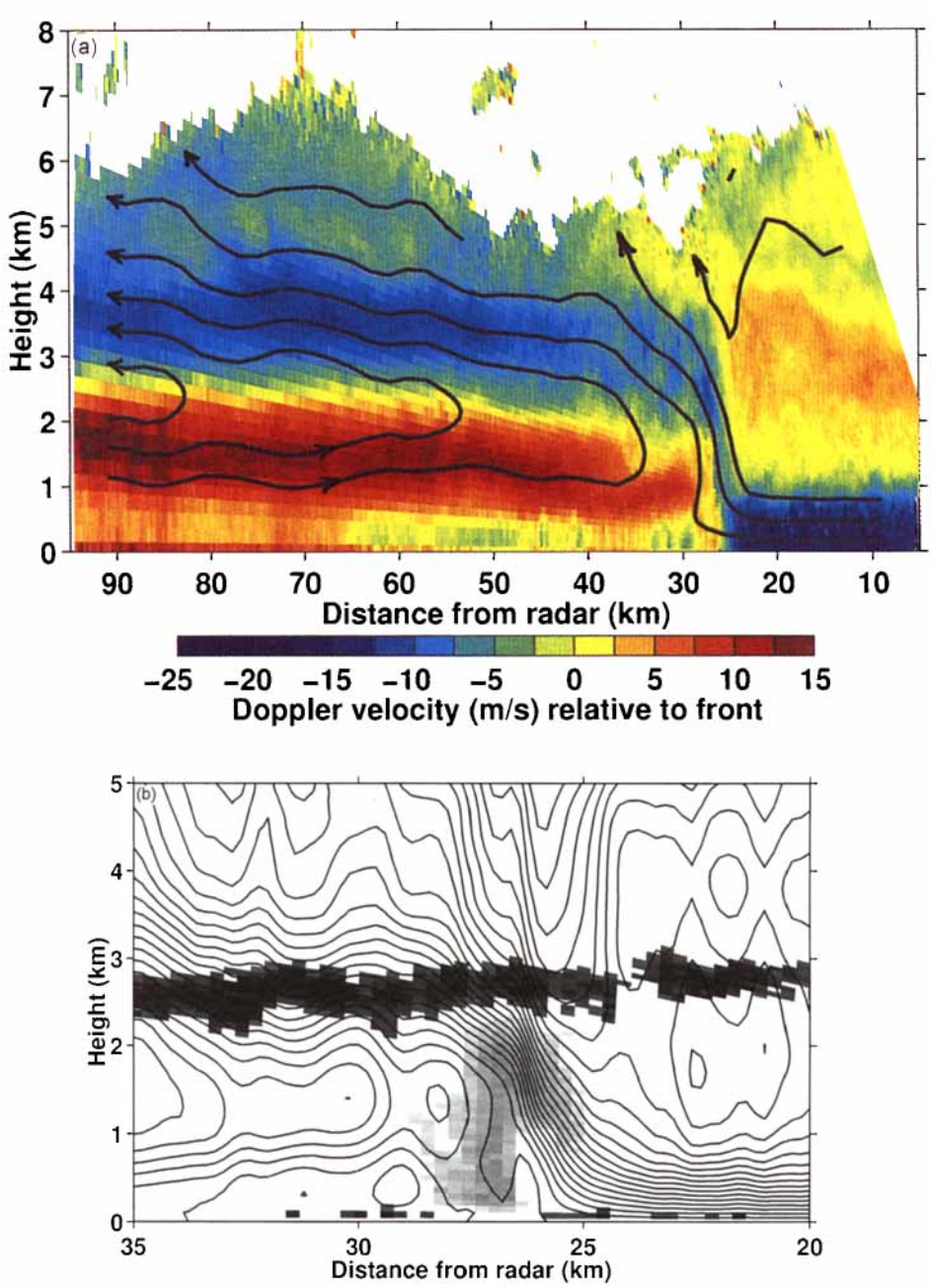

Figure 15. Cross-sections from the Chilbolton multi-parameter Doppler radar at right angles to cold front CF II at (a) and (b) 1839 UTC and (c) 1845 UTC on 24 October 1995. West is to the left and the front is travelling from left to right. The section in (a) corresponds to CD in Fig. 12(d) (part of AB in Fig. 10(c)). Colours in (a) show the transverse wind component relative to the front according to the scale at the foot of the figure. Solid curves in (a) are streamlines derived using a two-dimensional assumption. Solid curves in (b) and (c) are also streamlines but for an enlarged portion of the front near the line convection. Flux between adjacent streamlines in (a) and ((b) and (c)), respectively, is 5 and 1 kg s^{-1} per kilometre perpendicular to the diagrams. The pale shading in (b) and (c) shows radar reflectivity in the range 44 to 53 dBz. The darker shading represents the melting layer as inferred from values of linear depolarization ratio greater than −24 dB. The locations 'a', 'b' and 'c' in (c) are discussed in the text.

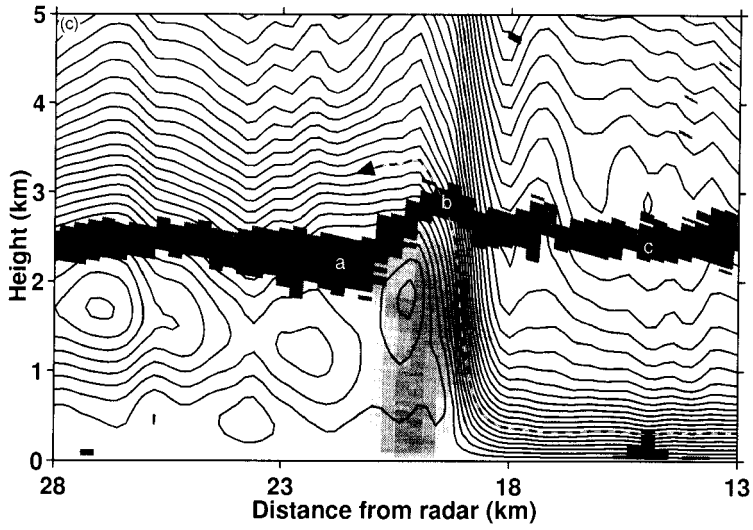

Figure 15. Continued.

instability, in the inflow to the line convection. This supports the prediction of potential instability in the vicinity of the line convection, given by the mesoscale model (Fig. 12(b)). (The corresponding θ_w lapse from the model is actually 15 to 14 °C.) Potential instability may not have existed at all times and places along the line convection, however, because there were times (e.g. Fig. 15(b)) when there was relatively little evidence of a bright-band undulation. Nevertheless, this emphasis on potential instability differs from that given by Browning and Pardoe (1973) who, whilst noting a small increase in θ_w very close to the surface, drew attention to the near-neutral stability (i.e. nearly constant θ_w and air nearly saturated) in the lowest 2.5 km just ahead of line convection. Browning and Pardoe used sequential radiosondes in their study and, although their sondes were well placed just ahead of the line convection, these sondes provided only single samples. It is possible, therefore, that patches of potential instability also occurred in some of their cases but that they were not detected. The existence of some potential instability in the inflow to CF II may be attributable to a vestigial dry intrusion associated with the remains of CF I (just as the much better-defined dry intrusion associated with CF II was situated just in advance of CF III).

6. Synthesis and conclusions

The archetypal mesoscale structure of an ana-cold front comprises a narrow cold-frontal rainband (NCFR) due to line convection embedded within a wide cold-frontal rainband (WCFR) due to slantwise ascent associated with a strong transverse-front mesoscale circulation (Browning 1990). Whereas most observational studies on the mesoscale have concentrated on this mature stage, the present paper has explored by means of a case-study how such a mature frontal system developed from pre-existing frontal features. The synoptic-scale context was one of frontal fracture accompanying rapid cyclogenesis (Shapiro and Keyser 1990). The cyclogenesis occurred on the cold side of the polar front ('instant occlusion' scenario as described by McGinnigle *et al.* (1988)) during which multiple new cold fronts approached the frontolysing polar front. We have examined the mesoscale and convective structure and evolution of these fronts, concentrating especially

on the way in which a dominant new (secondary) cold front merged with the frontolysing initial cold front. No generality is claimed for the particular evolution observed in this one case; rather, the aim of the investigation has been the more modest one of establishing the kinds of mesoscale substructure and interactions that may be important in this fairly common type of situation.

We have shown how the dominant secondary cold front (CF II) in this case started as a shallow rope cloud, indicative of a sharp convergence line within the boundary layer, and then evolved over the period 0000 to 1800 UTC as summarized in Fig. 16. At 0000 UTC in Fig. 16, CF II was situated a few hundred kilometers behind the main polar front, CF I. CF I was still active at 0000 UTC but by 0600 UTC it had largely frontolysed, leaving moist residues where its anvils had evaporated. As CF II approached the frontolysed cold front CF I at 1200 UTC, CF II was already producing an NCFR which soon developed into line convection. At this time CF II was not yet producing any obvious mesoscale (stratiform) cloud canopy of its own; however, it was surrounded by scattered outbreaks of rain related to deepening cloud areas associated with the moist residues of CF I, which over the new few hours developed as *rearward*-trailing cloud plumes associated with the re-invigorating CF I. Each of these plumes could be attributed to the renewed ascent of the patches of moist air (moist residues) left behind about 12 hours earlier by the decay of vigorous convective storm cells, with *forward*-trailing anvils, along the original polar front (CF I) before it began to frontolyse (Fig. 9). The change in the orientation of the CF I anvil plumes is indicative of a change from a kata- to a locally ana-frontal (direct) circulation. Over the period from just before 1200 to 1500 UTC, the development of this ana-circulation led to a broad and quite intense WCFR within which the CF II NCFR could be glimpsed in places. Then during the next 3 hours the CF II line convection itself intensified and it began to produce a stratiform cloud canopy of its own at mid-levels *beneath* the CF I plumes. By 1800 UTC the rearward-ascending outflow due to CF II had taken over as the major contributor to the ana-circulation and the predominant producer of precipitation in the WCFR.

Some aspects of the broad-scale thermodynamic structure and precipitation pattern were reasonably well represented by the Meteorological Office operational mesoscale model. One feature that was represented was the penetration of a finger of 'dry-intrusion' air with low θ_w just behind the front CF II where it became sharp at low levels. However, the model underestimated the strength of the rear-to-front component of relative flow within the dry intrusion and it failed to create the observed density current-like nature of the surface front. The model also generated a mesoscale canopy of moist ascent above the dry intrusion as observed but it failed to reproduce the strong front-to-rear relative flow ($> 10\ \mathrm{m\ s^{-1}}$) that was fed by the outflow from the line convection. A diagnosis of the model's shortcomings will be the subject of a later paper. The strong overall transverse circulation which the model poorly reproduced is evidently the key to the cold-frontal structure. It led to the development of a WCFR due to the creation of a combined rearward-ascending outflow from CF II and from the re-invigorated CF I.

The radar-observed rear-to-front wind component associated with the finger of low-θ_w dry-intrusion air behind CF II, leading to a density-current-like feature that forced warm boundary-layer air ahead of it to ascend in an organized way into the canopy of rearward-sloping mesoscale ascent, is regarded as archetypal. In such situations there may be a positive feedback process in which the cooling due to evaporation and melting of precipitation falling from the canopy into the dry finger (Clough and Franks 1991; Yang and Houze 1995) leads to an intensification of the mesoscale circulation which in turn leads to a tendency for sharpening of the surface front. However, the front in this case had produced a rope cloud indicative of a sharp surface convergence line even *before* the

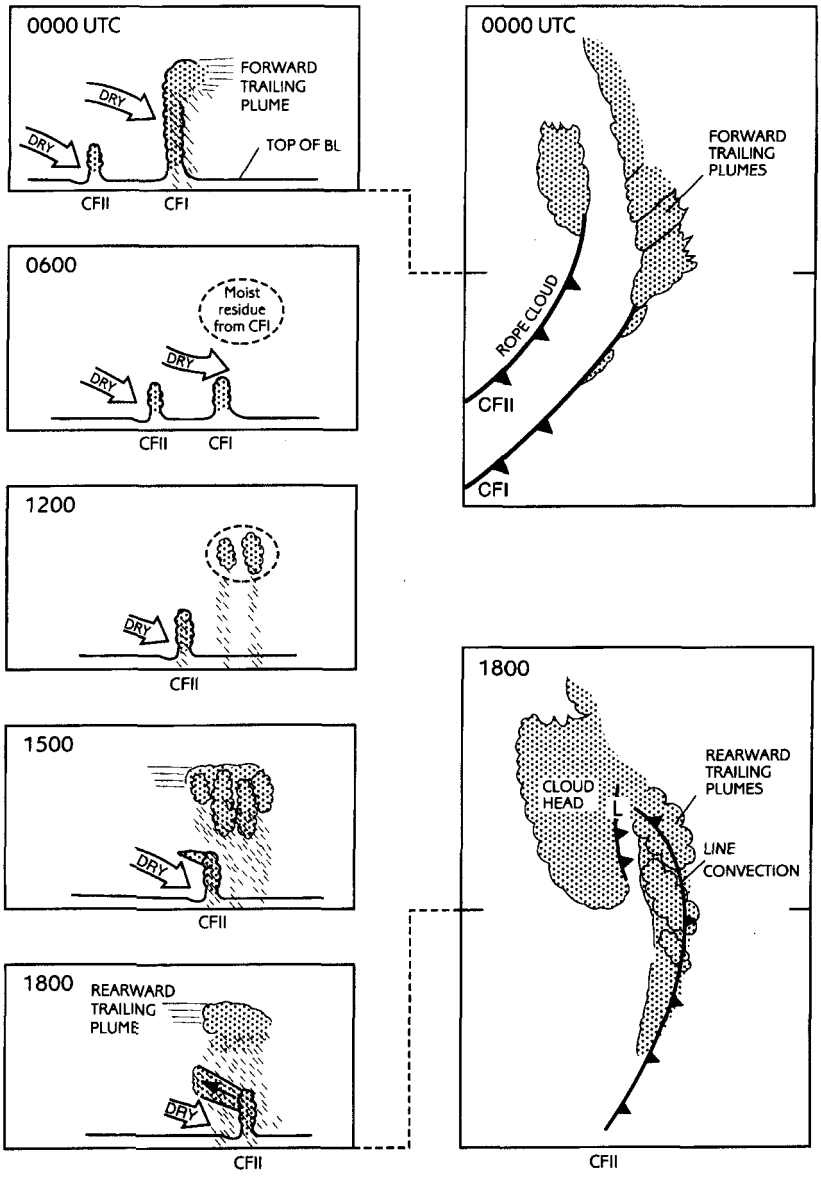

Figure 16. Schematic representation of the evolution of cloud and precipitation associated with cold fronts CF I and CF II during the period of cyclogenesis. Left side: cross-sections. Right side: plan views. Cloud is stippled and precipitation hatched. Open arrows denote dry intrusions: another arrow (1800 UTC only) represents saturated mesoscale ascent. The positions of the cross-sections for 0000 and 1800 UTC, respectively, are indicated on the two plan views. The diagrams are not drawn precisely to scale, although as a guide the west–east dimension of each frame is approximately 1500 km.

generation of extensive precipitation. Indeed this rope cloud went on to develop into an NCFR, with evidence of 2-dimensional line convection, again, just *before* the development of the WCFR associated with the mesoscale transverse circulation. The existence of the rope cloud possibly before the initiation of precipitation, together with the fact that the rear-to-front inflow was strongest at the trailing edge of the WCFR, suggests that the precipitation processes probably were *not* the primary factor in the development, and that

there may have been a mesoscale transverse circulation already in association with the dry intrusion when it first entered the region of cyclogenesis. An example of a mesoscale circulation in the dry air which was associated with a shallow rope-like cloud is given by Browning (1995).

The nature of the cold fronts upstream of the developing low centre in this study may be summarized as follows:

- Multiple cold fronts occurred within the dry-intrusion region before cyclogenesis.
- The early-stage cold fronts, with the exception of the initial one, were all observed as thin lines of, often rope-like, boundary-layer clouds beneath, and perhaps triggered by, the advancing dry intrusion(s).
- Before cyclogenesis the first cold front was producing a major polar-front cloud band, with embedded thunderstorms, but it underwent frontolysis before cyclogenesis as the dry-intrusion air overran it (kata-cold front structure).
- As cyclogenesis got underway the kata-cold frontal circulation was replaced by an ana-cold frontal circulation: this could be ascertained from the switch from forward-trailing to rearward-trailing convectively generated cloud plumes associated with the first cold front.
- Only two of the many cold fronts persisted as significant surface features during cyclogenesis. At the onset of the ana-circulation one of these developed intense line convection and a rearward-sloping stratiform canopy due to the strong transverse circulation.
- The strong transverse circulation associated with the dominant cold front appeared to be forced rather more by the large-scale dynamics than by precipitation-related mesoscale processes, although the relative importance of these processes probably varies from case to case.

Acknowledgements

We are grateful to John Goddard for provision of data from the Chilbolton radar, and to Danny Chapman for producing the cross-sections from it. The Chilbolton radar is part-funded as a facility of the Natural Environment Research Council.

References

AMS 1996 Proceedings of the seventh conference on mesoscale processes. Reading, September 1996. American Meteorological Society, Boston, Mass.

Bader, M. J., Forbes, G. S., Grant, J. R., Lilley, R. B. E. and Waters, A. J. 1995 *Images in weather forecasting*. Cambridge University Press

Bennetts, D. A. and Hoskins, B. J. 1979 Conditional symmetric instability—a possible explanation for frontal rainbands. *Q. J. R. Meteorol. Soc.*, **105,** 945–962

Browning, K. A. 1990 Organization of clouds and precipitation in extratropical cyclones. Pp. 129–153 in *Extratropical cyclones*. Eds. C. W. Newton and E. O. Holopainen. American Meteorological Society, Boston, Mass.

1995 On the nature of the mesoscale circulations at a kata-cold front, *Tellus*, **47A,** 911–919

Browning, K. A. 1997 Mesoscale aspects of extratropical cyclones: an observational perspective. In: Bergen post-conference book. Ed. M. Shapiro. American Meteorological Society, Boston, Mass. (In press)

Browning, K. A. and Pardoe, C. W. 1973 Structure of low-level jet streams ahead of mid-latitude cold fronts. *Q. J. R. Meteorol. Soc.*, **99,** 619–638

Browning, K. A. and Roberts, N. M. 1994 Structure of a frontal cyclone. *Q. J. R. Meteorol. Soc.*, **120,** 1535–1557